J. Vis. Commun. Image R. 59 (2019) 455–460

Contents lists available at ScienceDirect

J. Vis. Commun. Image R.

journal homepage: www.elsevier.com/locate/jvci

An efficient 3D face recognition approach using Frenet feature of iso-geodesic curves

Biao Shi, Huaijuan Zang, Rongsheng Zheng, Shu Zhan *

School of Computer and Information, Hefei University of Technology, Hefei 230009, China

ARTICLE INFO

Article history:
Received 4 June 2018
Revised 2 December 2018
Accepted 1 February 2019
Available online 2 February 2019

Keywords:
Facial curves
Frenet framework
3D face recognition
Iso-geodesic
Pose invariant

ABSTRACT

Extracting efficient features from the large volume of 3D facial data directly is extremely difficult in 3D face recognition (3D-FR) with the latest methods, which mostly require heavy computations and manual processing steps. This paper presents a computationally efficient 3D-FR system based on a novel Frenet frame-based feature that is derived from the 3D facial iso-geodesic curves. In terms of the evaluation of the proposed method, we conducted a number of experiments on the CASIA 3D face database, and a superior recognition performance has been achieved. The performance evaluation suggests that the pose invariance attribute of the features relieves the need of an expensive 3D face registration in the face preprocessing procedure, where we take less time to process conversely. Our experiments further demonstrate that the proposed method not only achieves competitive recognition performance when compared with some existing techniques for 3D-FR, but also is computationally efficient.

1. Introduction

Due to the natural and non-intrusive property of face data acquisition, automatic face recognition has many advantages when compared to other biometrics [24,26,45]. Correspondingly, researchers of computer vision [25,27,30,41,42] and pattern recognition [49–53] has obtained an increasing interest within the research field of computer vision over the past several decades. Despite recognition rates of advanced face recognition methods are quite high under constrained conditions, unfortunately, the rates can degrade crucially because of the pose changes, illumination variations and facial expression existed in images. With the rapid development of 3D sensors, many researchers have turned to 3D-FR. 3D data boost the face recognition by providing more detailed geometric information compared with conventional facial data. Unlike 2D images [43,46] or video [35,36,47], the recognition of 3D face is less affected by distortions. These benefits have led to advances in 3D-FR [1,2]. Although the rich geometric information of 3D face we can get, the 3D-FR also suffer from the problem of increased computation due to high dimensions of data. Manual selection of landmarks [1,3,5] or 3D to 2D projection techniques [2,4,6] are most commonly used to reduce the 3D facial data. However, the advantage of 3D over 2D data in recognition of the face may be limited by these data reduction methods.

Our work aims to take advantage of the inherent advantage of processing 3D data for 3D face recognition. Without projecting to 2D data, a set of novel features are extracted from the iso-geodesic curves [17] representation of 3D facial data. The Frenet geometric features [23] are faster to obtain which compared with the existing 3D point or surface-based representations. In [7], Sima has compared the computational cost of different 3D face representation methods.

The organization of the rest paper is as follows. Section 2 introduces related work in the area of 3D-FR. Section 3 presents the proposed noval techniques to obtain iso-geodesic curves from 3D facial data, then we illustrate the Frenet frame for the iso-geodesic curves [17] and the pose invariance property of its derivative geometric features by a series of mathematical formulas. An experimental performance evaluation in 3D-FR for the 3D facial data with illumination, expression, pose is provided in Section 4. Finally, Section 5 compares with the related work and concludes the findings.

2. Related work

A comprehensive survey about the 3D recognition methods have been showed in [7,8], In the following, we will review various methods for 3D-FR that are closely related to our work (Section 2.1). Afterwards, we introduce some challenges in 3D-FR (Section 2.2) and focus on the curve-based 3D face recognition method (Section 2.3).

* Corresponding author.
E-mail address: shu_zhan@hfut.edu.cn (S. Zhan).

https://doi.org/10.1016/j.jvcir.2019.02.002
1047-3203/

2.1. Three-dimensional face recognition

The goal of 3D face recognition can be coarsely summarized as finding the features [28] that are less affected by local variations such as pose, expressions, and occlusions. The approach to get the feature is grouped into three categories: feature-based, holistic and hybrid matching methods [7]. Feature-based matching method need finding similar features from special regions of the 3D face or the entire 3D face. Emambakhsh et al. generates planes using pairs of keypoints near the nose area, then the intersecting curves between planes are used to define features [2]. In holistic matching methods, most of them focus on the global similarity. A set of global features is used to described the entire face, for examples, the principle component analysis (PCA) method [9], the sighed shape difference map (SSDM) [10], region-based 3D deformable model (R3DM) [11]. The last approach [29] is established on the combination of the two methods mentioned above or the type of the data, in [13], 2.5D images are used to extract the keypoints.

2.2. Challenges in three-dimensional face recognition

Face recognition is an intense research area, since the numerous applications with it. Among these face recognition methods, it is divided into two-dimensional face recognition method and three-dimensional face recognition method depend on the type of the facial data. 3D facial data can provide more adequate and reliable geometric information than 2D image, but no one is perfect, 3D face recognition also needs face some challenges. Just like the acquisition of 3D facial data mostly suffers from losing information due to the rotation of the head out of plane. Additionally, variations in 3D facial data due to the degree of pose angel and changes in facial expressions will degrade face recognition performance. In order to overcome these challenges, Ocegueda et al. proposed a measure field to calculate the probability of each vertex of 3D facial data for 3D-FR and 3D facial expression recognition [14]. Yu et al. viewed the human face surface as a series of iso-geodesic curve sets taken from the tip of the nose and used dynamic programming to measure the similarity between two faces [15]. Recently, they found that only the subset of the vertex of the face mesh model contains sufficient information to distinguish the faces, according to this finding, the concept of three-dimensional sparse direction vertices is proposed [16]. However, feature extracted from large volume of 3D facial points involve heavy computations, furthermore, it is usually affected by facial expression easily.

2.3. Curve-based methods

These curve-based methods usually use a set of curves extracted from facial surface as features. They contain abundant geometrical information that come from different facial regions. Compared to point-based methods [12,13], the extraction or comparison of curve in large volume of facial data is computationally more efficient, and unlike surface-based methods [16], they do not provide global feature which need to expense high computational cost. Curve-based method have been also applied in [17–20]. In [18], Samir et al. proposed an iso-geodesic curve-based framework, then use a Riemannian analysis framework to compare these facial curves. Li et al. identified six rigid regions where the curves is extracted in 3D-FR [19]. Li and wang employed multiple facial curves, including ridge curves, center profile curves, and horizontal profile curves to get better performance [20], an extra 3D pose correction step is involved in the above-mentioned methods. However, the iso-geodesic curves proposed by Drira et al. [17], as one of the curves, originate at the tip of nose can be easily localized, extracted and compared with lower computational cost.

3. Proposed method

This section describes the proposed method that extracts the noval Frenet frame-based feature from the iso-geodesic curve representation of 3D facial data for 3D-FR, and the pose invariance property of the feature will be demonstrated. Our approach is a best of both worlds, on the one hand, it can represent a large amount of 3D facial data as a small feature space. On the other hand, it eliminates the step of face registration and reduces computational costs.

3.1. Preprocessing

The CASIA-3D [21] dataset used in this paper contains many undesired regions and noise, which has a great influence on the experiment. Therefore, a series of face preprocessing techniques is applied. With the development of computer vision, there are many ways to preprocess video and images [34,39,40,44,48]. In this paper, first, according to the position of the nose point provided by the dataset, we use the nose tip to create a 3D mask whose region is equal to the average 3D facial area, a pure 3D face can be obtained by the 3D mask. Then we employ a mean value method to smooth the coarse 3D facial surface and reduce the noise of the face region. Finally, filling out all holes on facial surface with an interpolation step. Fig. 1 shows some examples of the face preprocessing results.

3.2. 3D face normalization

Three-dimensional face point cloud data is nonuniform in three-dimensional space. These point clouds form a surface that can be represented by $z = f(x,y)$, this surface is a three-dimensional face, z represents the depth value at (x,y). We use a normalized method to uniformly insert the 3D face point cloud data into the square grid defined by the following boundary values.

$$[x_{min}, x_{max}] = \{x_1 \in \mathbb{R} : x_{min} \leqslant x_1 \leqslant x_{max}\} \tag{1}$$

$$[y_{min}, y_{max}] = \{y_1 \in \mathbb{R} : y_{min} \leqslant y_1 \leqslant y_{max}\} \tag{2}$$

Here, $[x_{min}, y_{min}], [x_{max}, y_{max}]$ are the coordinate values of the definitive three-dimensional face boundary, then we can calculate the $z_1 = f(x_1, y_1)$ of the given 3D facial data on the square grid. After the normalization step, we have a common topology to do the following work.

3.3. Extraction of iso-geodesic curves

Once the 3D face data is normalized, iso-geodesic curves can be extracted. Due to the regularization, the coordinates of the nose point provided by the dataset cannot be used, we can locate the nose point by detecting the maximum z value, and position the nose point to the origin of the uniform mesh to create a coordinate system and divide the mesh into four In the quadrant, any point in the four quadrant regions will have a corresponding depth z. Several such points will form a space curve. As shown in Fig. 2, these curves are iso-geodesic curves and can be represented by drawing spheres of different lengths of radius. Changing the length of the radius and the distance between each curve, we can get any area and any number of iso-geodesic curves. In this paper, in order to ensure that the recognition rate is not reduced, the calculation amount is reduced as much as possible, through experiments, it is found that extracting the 13 iso-geodesic curves of the average distribution of the 3D face can obtain the best recognition effect.

Fig. 1. Automatic preprocessing of a 3D face.

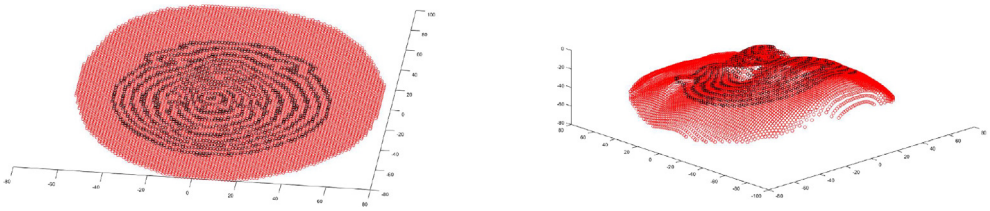

Fig. 2. Iso-geodesic curves of 3D face.

3.4. Frenet feature of iso-geodesic curves

Each extracted iso-geodesic curve is a spatial curve. According to each point of the curve, a local coordinate system consisting of three orthogonal basis vectors can be constructed. This coordinate system is called the Frenet frame. Suppose a space curve $\beta(s)$ of interval (a,b), in a rectangular coordinate system, $\beta(s)=(x(s),y(s),z(s))$, where $x(s)$, $y(s)$ and $z(s)$ are all functions of the arc-length variable s. Take n points in the interval (a,b):

$$c=\{a=s_0<s_1<\cdots<s_n=b\}. \tag{3}$$

The tangent vector at a point on the space curve (s) is:

$$\beta'(s)=\lim_{x\to 0}\frac{\beta_{s_i}-\beta_{s_{i-1}}}{\Delta s}. \tag{4}$$

Then we can get the unit length tangent vector T as:

$$\widehat{T}=\frac{\beta'(s)}{\|\beta'(s)\|} \tag{5}$$

$$\beta'(s)=\|\beta'(s)\|\widehat{T}. \tag{6}$$

The derivative of (6) is:

$$\beta''=\|\beta'\|'\widehat{T}+\widehat{T}'\|\beta'\|. \tag{7}$$

According to the definition, a vector with a certain length is orthogonal to its derivative, Since $\left|\widehat{T}\right|=1$, so it is orthogonal to $\widehat{T}'$ and the principal normal vector $\widehat{N}$ at this point, $\widehat{T}\cdot\widehat{N}=0,\widehat{T}'$ is proportional to $\widehat{N}$, so the formula can be transformed into:

$$\beta''=\|\beta'\|'\widehat{T}+\|\beta'\|^2\kappa\widehat{N}. \tag{8}$$

Where is the curvature at the point of the spatial curve, the subnormal vector $\widehat{B}$ as the third orthogonal vector can be obtained by $\widehat{B}=\widehat{T}\times\widehat{N}$, and these three mutually orthogonal vectors make up the basis vector of the feature, as shown in Fig. 3.

According to the distribution method of cross multiply:

$$\beta'\times\beta''=\kappa\|\beta'\|^3\widehat{B}. \tag{9}$$

Both sides of the equation in (9) are taken the magnitude:

$$\|\beta'\times\beta''\|=\kappa\|\beta'\|^3 \tag{10}$$

$$\kappa=\frac{\|\beta'\times\beta''\|}{\|\beta'\|^3}. \tag{11}$$

Substituting (11) into (9) gives:

$$\widehat{B}=\frac{\beta'\times\beta''}{\|\beta'\times\beta''\|}. \tag{12}$$

Similarly, the torsion ξ can be obtained:

$$\xi=\frac{\beta'\times\beta''\cdot\beta'''}{\|\beta'\times\beta''\|^2}. \tag{13}$$

We can know from the definition of the Frenet formula [22]:

$$\widehat{T}'=\kappa\widehat{N} \tag{14}$$

$$\widehat{N}'=\xi\widehat{B}-\kappa\widehat{T} \tag{15}$$

$$\widehat{B}'=-\xi\widehat{N}. \tag{16}$$

Their magnitude are:

$$\left\|\widehat{T}'\right\|=\kappa \tag{17}$$

$$\left\|\widehat{N}'\right\|=\sqrt{\kappa^2+\xi^2} \tag{18}$$

$$\left\|\widehat{B}'\right\|=\xi. \tag{19}$$

We can obtain the magnitude of the change of the base vector for each point on each curve by using Eqs. (18)–(20), and then calculate the average of these three types of values for all points on each curve, denoted as F_ξ, F_N, F_κ, as the feature of the space curve:

$$F_\kappa=\frac{1}{N}\sum_{i=1}^{N}\kappa(s_i) \tag{20}$$

$$F_n=\frac{1}{N}\sum_{i=1}^{N}\sqrt{\kappa(s_i)^2+\xi(s_i)^2} \tag{21}$$

$$F_\xi=\frac{1}{N}\sum_{i=1}^{N}\xi(s_i). \tag{22}$$

Here F_κ is the average curvature of each point on this curve, F_ξ is the average torsion of each point, F_n is the average rate of change of the principal normal vector at each point, and curvature and torsion describe how the space curve transitions along its path and distortion. In addition to the three kinds of feature of the three elements of Frenet, the length of the curve can also be used as a fea-

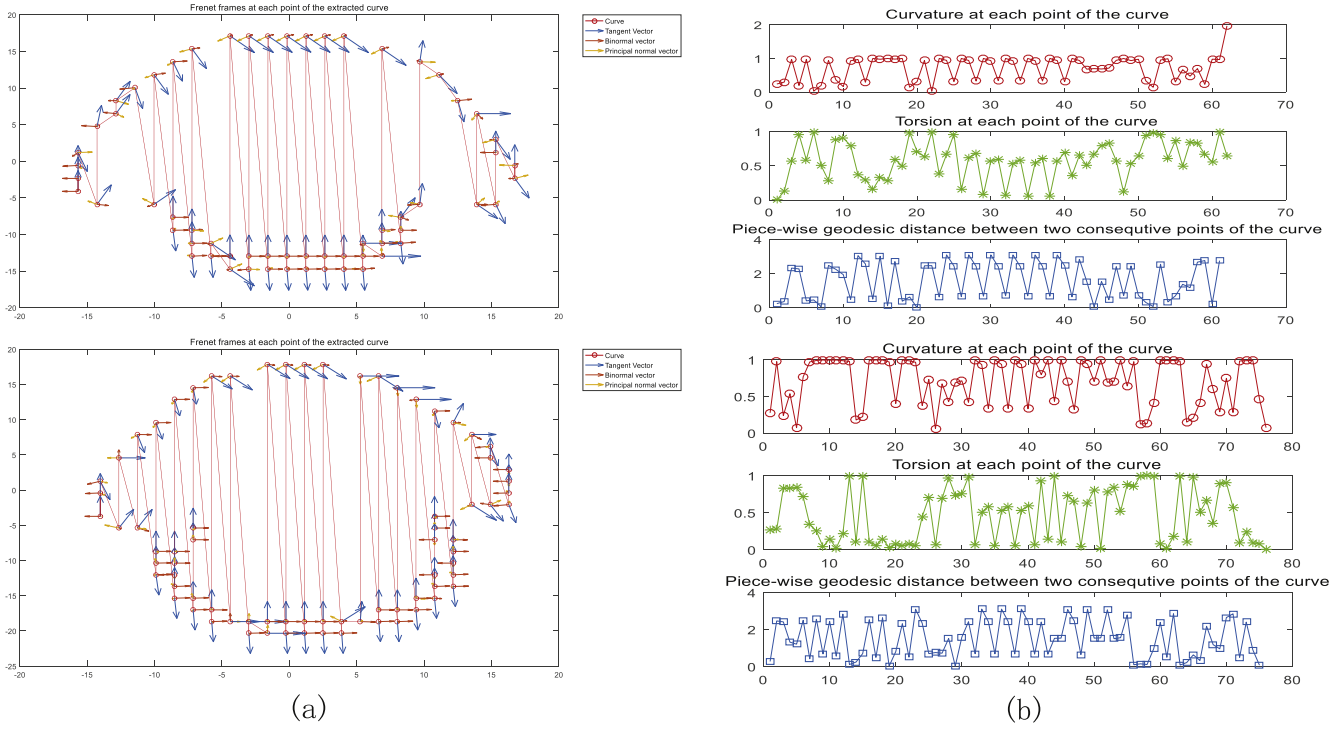

Fig. 3. (a) Frenet frames at each point of the extracted curve; (b) Curvature, Torsion at each point and consecutive points geodesic distance.

ture that is not affected by pose and expressions. Because the space curves belong to the Riemannian manifold, they can be calculated by two adjacent consecutive points on the same curve. The tangent vector of $[i,j]$ is used to calculate the arc length between two points. Known unit tangent vector β_i', β_j', then we can get the angle of these two tangent vectors by the following formula:

$$cos\delta = \frac{\beta_i' \cdot \beta_j'}{\left|\beta_i'\right|\left|\beta_j'\right|} \tag{23}$$

$$\delta = arccos\left(\beta_i' \cdot \beta_j'\right). \tag{24}$$

Since δ is used as the angle between two consecutive point-cut vectors, δ is also a feature that is invariant to the pose, and all δ are summed to obtain F_δ:

$$F_\delta = \sum_{i=1}^{N} \delta(s_i). \tag{25}$$

Each iso-geodesic curve will be extracted from the four kinds of features of (20)–(22) and (25), because each feature takes the average or sum of the eigenvalues of each point on iso-geodesic curve. Therefore, the changes of some regions have less influence on the feature of this curve, which reduces the interference of gestures, illumination, and expression when 3D face recognition is performed. The overall algorithm flow is shown in Fig. 4.

4. Experiment and result

In order to evaluate the universality and pose invariance of the features proposed in this paper, we select five different facial expression models (smile, laugh, angry, surprised, and closed eyes), ten different gesture models (Positive two, left and right upper and lower 20—30°, left and right up and down 50—60°, oblique right 20—30°, oblique left 50—60°), and five different lighting conditions (natural light, upper light, lower light, left light, right light) models of 123 people in the CASIA-3D face database as experimental data. When verifying the generality of features under different lighting conditions, the three-dimensional human faces under five different illuminations are selected as testing sets, and the remaining three-dimensional human faces and two frontal three-dimensional human faces under the four lighting conditions are taken as training sets. When verifying the generality of features under different lighting conditions, first, we choose the three-dimensional face in any kind of lighting conditions as a testing set, and then use three-dimensional face in other lighting conditions as a training set. Then verifying the feature's expression and pose invariance, this paper will select five different lighting three-dimensional faces and two front three-dimensional faces as the training set, and three-dimensional faces of various expressions and poses as the testing set.

To enable the classifier to classify these nonlinear features, two subspace projection techniques are used: PCA and LDA. The sub-

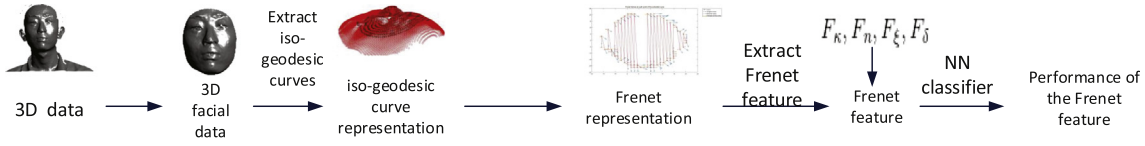

Fig. 4. The proposed method architecture.

Table 1
3D-FR performance for different features using PCA subspace projection technique.

Feature	Illumination	Expression	20—30°	50—60°
F_κ	88	67	57	33
F_n	52	41	30	16
F_ξ	46	32	21	10
F_δ	90	76	65	40

Table 2
3D-FR performance for different features using LDA subspace projection technique.

Feature	Illumination	Expression	20—30°	50—60°
F_κ	89	70	58	35
F_n	54	45	30	20
F_ξ	38	26	16	8
F_δ	92	80	68	42

space projection model is trained first with the features extracted from the training set, and then the features in the test set are projected and selected through this model because the minimum distance classifier (NN) can effectively classify the projection features of the test set. In this paper, NN is used to test and train the subspace projection features of 3D face recognition. The distance of NN selects the Euclidean distance. The final experimental results are shown in Tables 1 and 2, and the evaluation criteria is Rank-1 recognition rate.

5. Conclusion

We proposed a noval Frenet geometric feature of the iso-geodesic curves extracted from 3D facial data which can be used in the 3D-FR, and the performance of it have been evaluated from the above experiment, and the different proposed features have different performance in 3D-FR. In general, the sum of two adjacent consecutive tangent vectors angel as the feature F_δ perform the best even under pose distortion, and the feature F_κ also can provide complete geometric information about the 3D face. These two features are both computed from the tangent vector which suggests that the iso-geodesic curves generate a measurement of curvature. The other two features that is derived from the binomial and principal normal vectors provide nothing about discriminative attributes for 3D face recognition. We can find that only the curvature feature of the iso-geodesic curves extracted from 3D facial data can get good result because of the attributes of the curve.

Table 3 compares the result of 3D-FR using the CASIA-3D data set, which suggest that our method have better or comparable 3D-FR performance when compared with other methods listed in the table. In Table 4, we summarized the advantages of our proposed technique over the processing steps and the limitation of other methods. In the future work, we will continue to improve the recognition performance of this feature under a large posture and its efficiency. And I believe that the Frenet feature proposed in this article will be applied in the field of computer vision such as video [31–33] and image [37,38].

Table 3
Comparison of 3D-FR using the CASIA-3D dataset (“e: expression”, “n: neutral”, “i: illumination”).

Methods	Rank-1 recognition rate	Computation cost per 3D facial data in seconds
Li et al. [29]	e:85%	3.00 s with 3.0 GHz CPU
X. Wang [30]	n:91%	9.00 s with 2.64 GHz CPU
Y. A. Li [31]	n:91%	9.58 with 2.64 GHz CPU
Ours	e:91% i:94%	0.76 s with 2.64 GHz CPU

Table 4
Advantages of the proposed framework compared with existing methods.

Steps	Existing approaches	Limitations of these approaches	Our approach
Feature extraction	Manual landmarks or segments [23–25]	Not automatic	Automatic
Dimension reduction	2D projection [6,26]	Pose distortion	Direct extraction from 3D facial data
Computation complexity	complex processing [26]	Real-time application	Light computation
Matching	ICP-based [27,28,19]	Expensive	Not needed, Pose invariant

Conflict of interest

There is no conflict of interest.

Acknowledgements

This work was supported by National Nature Science Foundation of China Grand No: 61371156. The authors would like to thank the anonymous reviews for their helpful and constructive comments and suggestions regarding this manuscript.

References

[1] F.M. Sukno, J.L. Waddington, P.F. Whelan, 3-D facial landmark ization with asymmetry patterns and shape regression from incomplete features, IEEE Trans. Cybern. 45 (9) (2017) 1717–1730.
[2] M. Emambakhsh, A. Evans, Nasal patches and curves for expression-robust 3D face recognition, IEEE Trans. Pattern Anal. Mach. Intell. 39 (5) (2016) 995–1007.
[3] S. Elaiwat, M. Bennamoun, F. Boussaid, et al., A Curvelet-based approach for textured 3D face recognition, Pattern Recogn. 48 (4) (2015) 1235–1246.
[4] G. Sandbach, S. Zafeiriou, M. Pantic, Binary Pattern Analysis for 3D Facial Action Unit Detection, Bmva Press, 2012.
[5] A.J.M.A. Markus, A. Wollstein, C. Ruff, et al., An automatic 3D facial landmarking algorithm using 2D gabor wavelets, IEEE Trans. Image Process. 25 (2) (2015) 580–588.
[6] A. Savran, B. Sankur, M.T. Bilge, Comparative evaluation of 3D vs. 2D modality for automatic detection of facial action units, Pattern Recogn. 45 (2) (2012) 767–782.
[7] S. Soltanpour, B. Boufama, Q.M.J. Wu, A survey of local feature methods for 3D face recognition, Pattern Recogn. 72 (2017).
[8] K.W. Bowyer, K. Chang, P. Flynn, A survey of 3D and multi- modal 3D+2D face recognition, in: International Conference on Pattern Recognition, 2004.
[9] T. Russ, C. Boehnen, T. Peters, 3D face recognition using 3D alignment for PCA, in: IEEE Computer Society Conference on Computer Vision and Pattern Recognition, IEEE Computer Society, 2006, pp. 1391–1398.
[10] Y. Wang, J. Liu, X. Tang, Robust 3D face recognition by shape difference boosting, IEEE Trans. Pattern Anal. Mach. Intell. 32 (10) (2010) 1858–1870.
[11] S.Z. Gilani, A. Mian, P. Eastwood, Deep, Dense and Accurate 3D Face Correspondence for Generating Population Specific Deformable Models, Elsevier Science Inc., 2017.
[12] A.S. Mian, M. Bennamoun, R. Owens, Keypoint detection and feature matching for textured 3D face recognition, Int. J. Comput. Vision 79 (1) (2008) 1–12.
[13] M. Mayo, E. Zhang, 3D Face Recognition Using Multiview Keypoint Matching, 2009.
[14] O. Ocegueda, T. Fang, K. Shah S, et al., 3D face discriminant analysis using Gauss-Markov posterior marginals, IEEE Trans. Pattern Anal. Mach. Intell. 35 (3) (2013) 728–739.
[15] X. Yu, Y. Gao, J. Zhou, 3D face recognition under partial occlusions using iso-geodesic strings, in: IEEE International Conference on Image Processing, IEEE, 2016, pp. 3016–3020.
[16] X. Yu, Y. Gao, J. Zhou, Sparse 3D directional vertices vs continuous 3D curves: efficient 3D surface matching and its application for single model face recognition, Pattern Recogn. 65 (2017) 296–306.
[17] C. Samir, A. Srivastava, M. Daoudi, Three-Dimensional Face Recognition Using Shapes of Facial Curves, IEEE Computer Society, 2006.
[18] C. Samir, A. Srivastava, M. Daoudi, et al., An intrinsic framework for analysis of facial surfaces, Int. J. Comput. Vision 82 (1) (2009) 80–95.
[19] X. Li, F. Da, Efficient 3D Face Recognition Handling Facial Expression and Hair Occlusion, Butterworth-Heinemann, 2012, pp. 350–358.
[20] Y. Li, Y.H. Wang, J. Liu, et al., Expression-insensitive 3D face recognition by the fusion of multiple subject-specific curves, Neurocomputing (2017).
[21] CASIA-3D FaceV1 [on curve]. Available: http://biometrics.idealtest.org/.

[22] S. Zucker, Differential geometry from the Frenet point of view: boundary detection, stereo, texture and color, in: Handbook of Mathematical Models in Computer Vision, Springer US, 2006, pp. 357–373.
[23] M.L. Koudelka, M.W. Koch, T.D. Russ, A prescreener for 3D face recognition using radial symmetry and the hausdorff fraction, in: IEEE Computer Society Conference on Computer Vision and Pattern Recognition, IEEE Computer Society, 2005, p. 168.
[24] X. Lu, A.K. Jain, D. Colbry, Matching 2.5D face scans to 3D models, IEEE Trans. Pattern Anal. Mach. Intell. 28 (1) (2005) 31–43.
[25] M. Song, D. Tao, S. Sun, et al., Robust 3D face landmark localization based on local coordinate coding, IEEE Trans. Image Process. A Publ. IEEE Signal Process. Soc. 23 (12) (2014) 5108.
[26] O. Ocegueda, T. Fang, S.K. Shah, et al., 3D face discriminant analysis using Gauss-Markov posterior marginals, IEEE Trans. Pattern Anal. Mach. Intell. 35 (3) (2013) 728–739.
[27] K.I. Chang, K.W. Bowyer, P.J. Flynn, Multiple Nose Region Matching for 3D Face Recognition under Varying Facial Expression, IEEE Computer Society, 2006.
[28] T.C. Faltemier, K.W. Bowyer, P.J. Flynn, A region ensemble for 3-D face recognition, IEEE Trans. Inform. Forens. Secur. 3 (1) (2008) 62–73.
[29] L. Li, C. Xu, W. Tang, et al., 3D face recognition by constructing deformation invariant image, Pattern Recogn. Lett. 29 (10) (2008) 1596–1602.
[30] X. Wang, Q. Ruan, Y. Ming, 3D Face recognition using Corresponding Point Direction Measure and depth local features, in: IEEE International Conference on Signal Processing, IEEE, 2010, pp. 86–89.
[31] Y.A. Li, Y.J. Shen, G.D. Zhang, et al., An efficient 3D face recognition method using geometric features, in: International Workshop on Intelligent Systems and Applications, IEEE, 2010, pp. 1–4.
[32] H.Q. Zeng, X.L. Wang, C.H. Cai, J. Chen, Y. Zhang, Fast multiview video coding using adaptive prediction structure and hierarchical mode decision, IEEE Trans. Circ. Syst. Video Technol. (2014).
[33] H.Q. Zeng, K.-K. Ma, C.H. Cai, Fast mode decision for multi-view video coding using mode correlation, IEEE Trans. Circ. Syst. Video Technol. (2011).
[34] Y.T. Wang, J.B. Gong, D.Z. Zhang, C.Q. Gao, J.W. Tian, H.Q. Zeng, Large disparity motion layer extraction via topological clustering, IEEE Trans. Image Process. (2011).
[35] H.Q. Zeng, K.-K. Ma, C.H. Cai, Hierarchical intra mode decision for H.264/AVC, IEEE Trans. Circ. Syst. Video Technol. (2010).
[36] H.Q. Zeng, C.H. Cai, K.-K. Ma, Fast mode decision for H.264/AVC based on macroblock motion activity, IEEE Trans. Circ. Syst. Video Technol. (2009).
[37] Chen Wang, Kai-Kuang Ma, Feature histogram equalization for feature contrast enhancement, J. Vis. Commun. Image Represent. 26 (2015) 255–264.
[38] Chen Wang, Kai-Kuang Ma, Bipartite graph-based mismatch removal for wide-baseline image matching, J. Vis. Commun. Image Represent. 25 (6) (2014) 1416–1424.
[39] Chen Wang, Kai-Kuang Ma, Common visual pattern discovery via directed graph, IEEE Trans. Image Process. 23 (3) (2014) 1408–1418.
[40] Zhe Wei, Kai-Kuang Ma, Contrast-guided image interpolation, IEEE Trans. Image Process. 22 (11) (2013) 4271–4285.
[41] Zhe Wei, Kai-Kuang Ma, CanhuiCai, Prediction-compensated polyphase multiple description image coding with adaptive redundancy control, IEEE Trans. Circ. Syst. Video Technol. 22 (3) (2012) 456–478.
[42] Jing Tian, Kai-Kuang Ma, A survey on super-resolution imaging (in the special issue on video restoration and enhancement: algorithms and applications), in: Signal, Image and Video Processing, First Quarter, Springer Verlag, 2011.
[43] Turgay Celik, Kai-Kuang Ma, Multi-temporal image change detection using undecimated discrete wavelet transform and active contours, IEEE Trans. Geosci. Remote Sens. 49 (2) (2011) 706–716.
[44] Baojiang Zhong, Kai-Kuang Ma, On the convergence of planar curves under smoothing, IEEE Trans. Image Process. 19 (8) (2010) 2171–2189.
[45] Jing Tian, Kai-Kuang Ma, Stochastic super-resolution image reconstruction, J. Vis. Commun. Image Represent. 21 (3) (2010) 232–244.
[46] Turgay Celik, Kai-Kuang Ma, Unsupervised change detection for satellite images using dual-tree complex wavelet transform, IEEE Trans. Geosci. Remote Sens. 48 (3, Part 1) (2010) 1199–1210.
[47] Shaoshuai Gao, Kai-Kuang Ma, Error-resilient H.264/AVC video transmission using two-way decodable variable length data block, IEEE Trans. Circ. Syst. Video Technol. 20 (3) (2010) 340–350.
[48] Xuwei Wang, Kai-Kuang Ma, Noise adaptive rational filter, in: Signal, Image and Video Processing, vol. 4, issue 1, Springer Verlag, 2010.
[49] Baojiang Zhong, Kai-Kuang Ma, Wenhe Liao, Scale-space behavior of planar-curve corners, IEEE Trans. Pattern Recogn. Mach. Intell. 31 (8) (2009) 1517–1524.
[50] Jing Tian, Kai-Kuang Ma, A state-space super-resolution approach for video reconstruction, in: Signal, Image and Video Processing, vol. 4, issue 3, Springer Verlag, 2009, pp. 217–240.
[51] Zheng Wu, Ming-Yi He, Kai-Kuang Ma, Dilation-run wavelet image coding, in: Signal, Image and Video Processing, vol. 2, issue 2, Springer Verlag, 2008.
[52] Ju Han, Kai-Kuang Ma, Rotation invariant and scale-invariant gabor features for texture image retrieval, Image Vis. Comput. 25 (9) (2007) 1474–1481.
[53] Canhui Cai, Jing Chen, Kai-Kuang Ma, Sanjit K. Mitra, Multiple description wavelet coding with dual decomposition and cross packetization, in: Signal, Image and Video Processing, vol. 1, issue 1, Springer Verlag, 2007, pp. 53–61.